2006

Mineralogical characterization of protolith and fault rocks from the SAFOD Main Hole

John G. Solum
U.S. Geological Survey

Stephen H. Hickman
U.S. Geological Survey

David A. Lockner
U.S. Geological Survey

Diane E. Moore
U.S. Geological Survey, dmoore@usgs.gov

Ben A. van der Pluijm
University of Michigan - Ann Arbor

See next page for additional authors

GEOPHYSICAL RESEARCH LETTERS, VOL. 33, L21314, doi:10.1029/2006GL027285, 2006

Mineralogical characterization of protolith and fault rocks from the SAFOD Main Hole

John G. Solum,[1] Stephen H. Hickman,[1] David A. Lockner,[1] Diane E. Moore,[1] Ben A. van der Pluijm,[2] Anja M. Schleicher,[2] and James P. Evans[3]

Received 19 June 2006; revised 7 August 2006; accepted 6 October 2006; published 9 November 2006.

[1] Washed cuttings provide a continuous record of the rocks encountered during drilling of the main hole of the San Andreas Fault Observatory at Depth (SAFOD). Both protolith and fault rocks exhibit a wide variety of mineral assemblages that reflect variations in some combination of lithology, P-T conditions, deformation mechanisms, and fluid composition and abundance. Regions of distinct neomineralization bounded by faults may record alteration associated with fluid reservoirs confined by faults. In addition, both smectites occurring as mixed-layer phases and serpentine minerals are found in association with active strands of the San Andreas Fault that were intersected during drilling, although their rheological influence is not yet fully known. Faults containing these mineralogical phases are prime candidates for continuous coring during Phase 3 of SAFOD drilling in the summer of 2007. **Citation:** Solum, J. G., S. H. Hickman, D. A. Lockner, D. E. Moore, B. A. van der Pluijm, A. M. Schleicher, and J. P. Evans (2006), Mineralogical characterization of protolith and fault rocks from the SAFOD Main Hole, *Geophys. Res. Lett.*, *33*, L21314, doi:10.1029/2006GL027285.

1. Introduction

[2] The San Andreas Fault Observatory at Depth (SAFOD) Main Hole, drilled near Parkfield, California in 2004 and 2005 as part of the National Science Foundation's EarthScope Project, provides the unique opportunity to obtain in-situ samples from active traces of the San Andreas Fault (SAF) system [*Hickman et al.*, 2004]. These samples help address long-standing issues such as the causes of the apparent weakness of the SAF [*Lachenbruch and Sass*, 1992; *Zoback*, 2000], the mechanical involvement of fluids in the faulting process [*Hickman et al.*, 1995] and the processes that control seismogenic vs. creeping behavior. Multiple faults were recognized during drilling of SAFOD, five of which are discussed below. The objectives of this first systematic study of mineralogy are to: 1) divide the SAFOD Main Hole into mineralogical zones, with boundaries likely to be major faults, 2) characterize the mineral assemblages of fault rocks, the active SAF in particular, as a first step toward understanding frictional and geochemical properties and fault evolution, and 3) identify candidate zones for continuous coring that will be sampled during Phase 3 drilling in 2007.

2. Methods

[3] The SAFOD borehole was drilled to a total measured depth of 3997 m in 2004 and 2005 (see http://www.icdp-online.de/sites/sanandreas/index/). All depths reported in this paper are along hole measured depth (MD), and not true vertical depth (TVD). Drill cuttings were collected at 3 m intervals, and were gently washed in tap water in a 140-mesh sieve (0.106 mm) to remove drilling mud. Material that did not pass through the sieve was air dried at room temperature and is hereafter referred to as washed cuttings. Sub-samples were collected from archived washed cuttings using a mechanical chute-type sample splitter to preserve representative mineralogy and then crushed until they passed through a 190 μm mesh. Samples were analyzed using X-ray diffraction (XRD) techniques (CuKα radiation, 2–65 °2θ with a step size of 0.02 °2θ and a count time of 2 seconds) at 30 m intervals from 1219 to 3048 m, at 15 m intervals from 3048–3780 m, and at 3 m intervals across major lithologic boundaries and fault zones. Two samples from a clay-rich shear zone sampled by a spot core at 3067 m were also analyzed.

[4] Peak areas, a proxy for mineral concentration, were measured for all phases, and peak widths, a function of crystallite size, were measured for phyllosilicate phases [see *Solum and van der Pluijm*, 2004]. Quantitative XRD analysis was conducted on samples from five fault zones penetrated by SAFOD.

[5] Cuttings collected during drilling provide a continuous record of lithology, however there are issues that must be addressed when using cuttings to characterize mineralogy. These include: loss of formation clays during washing; difficulty resolving small features (i.e., thin beds, veins, or faults) because cuttings are an average of rock types over a 3-m-long interval; mixing as cuttings travel from the drill bit to the surface, especially in inclined holes where a cuttings bed may develop on the low side of the hole; and contamination of cuttings derived at the drill bit by borehole collapse and abrasion further up the hole. In addition, XRD cannot reliably quantify phases present at less than a few weight percent, nor does it provide information about textures or cross-cutting relationships. These types of detailed analyses are best performed using optical thin section observations [*Barton et al.*, 2005] or electron microscopy [*Schleicher et al.*, 2006]. In spite of these limitations, XRD analysis is ideally suited to the systematic characterization of mineralogy in the protolith and SAF rocks penetrated by the SAFOD hole.

[1]Earthquake Hazards Team, U.S. Geological Survey, Menlo Park, California, USA.
[2]Department of Geological Sciences, University of Michigan, Ann Arbor, Michigan, USA.
[3]Department of Geology, Utah State University, Logan, Utah, USA.

0094-8276/06/2006GL027285$05.00

[6] For the purpose of the present study, faults were identified based on juxtaposition of significantly different lithologies, the presence of pervasively sheared mineral surfaces recognized optically, or variations in physical properties as inferred from geophysical logs. The sampled faults are (Figure 1): 1) a fault separating granite from granodiorite (1360–1450 m), which likely correlates with a shear zone identified in the SAFOD Pilot Hole by *Boness and Zoback* [2004], 2) a fault separating granodiorite from brecciated sandstones and shales (1926–1935 m), 3) a fault separating sandstone from interbedded sandstones and shales (2545–2560 m), 4) a pervasively sheared fault sampled during coring at the end of Phase 1 (3067 m), and 5) a fault zone associated with distinctive mineral assemblages and ongoing casing deformation (3300–3353 m [see *Zoback et al.*, 2005]). As discussed by *Boness and Zoback* [2005, 2006], faults 1–3 were identified on the basis of physical property variations seen in geophysical well logs, preliminary on-site cuttings analyses, and changes in bedding attitude from wellbore image logs. All faults hereafter are referred to by the top of their depth range.

3. Results

[7] A summary diagram with mineral assemblages is shown in Figure 1. The occurrence and characterization of diagnostic minerals in the SAFOD Main Hole are discussed below. The primary phases that are used to define mineralogical zones (separated by red dashed lines in Figure 1) are chlorite, illite, illite-smectite, laumontite, hornblende and serpentine. Quartz and feldspars are ubiquitous, and are not as useful in defining mineralogical zones.

3.1. Granite and Granodiorite

[8] The mineralogical survey discussed in this paper begins in a granite at 1200 m MD. The granite is in fault contact with a granodiorite at ~1400 m MD, which persists to 1920 m MD. For our purposes these igneous rocks are grouped into a single package of granitic rocks. The primary phases in this package are quartz, undifferentiated feldspars, biotite, and hornblende in the granodiorite. Chlorite and laumontite are the dominant alteration phases.

3.2. Arkosic Sediments

[9] The hole encountered a sequence of arkosic sedimentary rocks at 1920 m MD, with interbedded shales and siltstones. This sequence persists to 3150 m MD, and is composed of three distinct zones. The first extends from 1920 to 2550 m MD. This zone is dominated by quartz, feldspars and illite with minor laumontite and hornblende in its upper portion. The concentration of chlorite in this zone is highly variable. The second zone extends from 2550 to 2720 m MD, and is recognized by the occurrence of a mixed-layer illite-smectite phase. It is difficult to fully characterize I-S using routine bulk rock analyses due to potential contamination by drilling mud (montmorillonite), and the need to solvate the samples with ethylene glycol to identify smectitic clays. Therefore, the objective of this paper is only to recognize the presence of such phases, not to fully characterize them, which is the focus of future study. The second zone also contains quartz and feldspars, and is enriched in chlorite and illite. The first and second

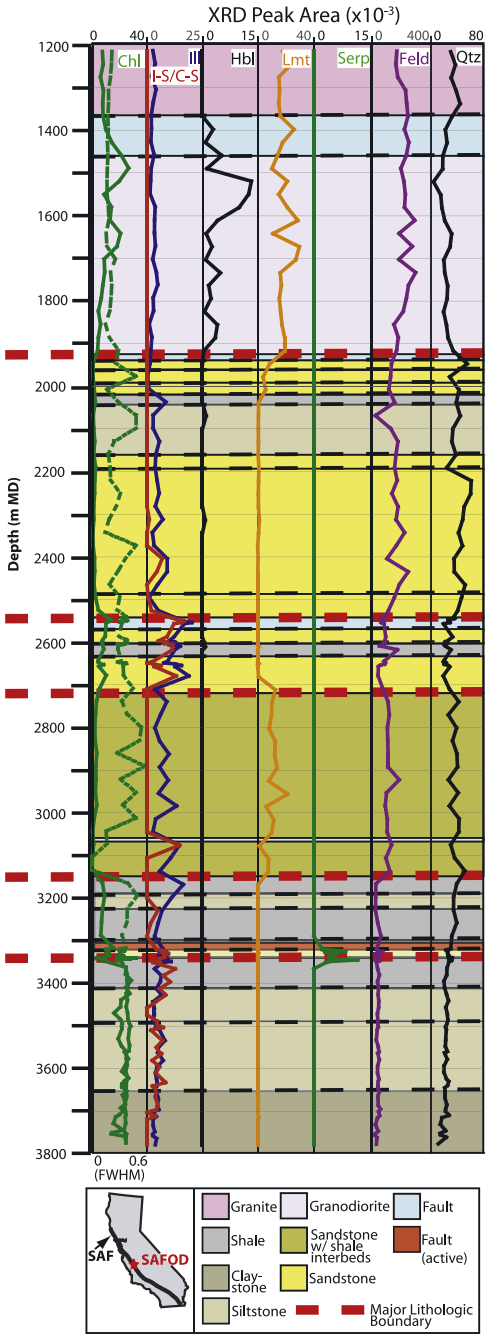

Figure 1. Relative mineral abundances from the SAFOD main hole obtained from peak areas on XRD powder patterns. Crystallinity, represented by full-width at half-maximum (FWHM) in units of degrees, is also shown for chlorite as a dashed line. Minerals are chlorite (chl), illite (ill), mixed-layer illite-smectite and chlorite-smectite (i-s/c-s), hornblende (hbl), laumontite (lmt), serpentine (serp), undifferentiated feldspars (feld) and quartz (qtz). Major lithologic boundaries (from *Boness and Zoback* [2006]) are shown by dashed lines. Boundaries between major mineralogical zones are given by dashed red lines. Location of the SAFOD hole shown as a star on the inset location map. SAF on inset map denotes active trace of the San Andreas Fault.

zones are separated by a prominent fault (discussed below). The third zone extends from 2720 to 3150 m MD, exhibits an increased proportion of interbedded shales and is recognized by the occurrence of abundant laumontite and an increased amount of illite. This zone also contains quartz, feldspars, and minor chlorite.

3.3. Shales/Siltstones

[10] A sequence of shales, siltstones and claystones was encountered at 3150 m MD and persists to the bottom of the XRD survey at 3800 m MD. This sequence is composed of two distinct zones. The first extends from 3150 to 3350 m MD, while the second is from 3350–3800 m MD. Both zones are dominated by chlorite, quartz, and feldspars. The chlorite concentration is significantly greater in the second zone than in the first. The chlorite peak widths (a function of the size of the X-ray scattering domain) are relatively constant in both zones, suggesting both chlorite populations are related.

3.4. Serpentine Minerals

[11] Minor amounts (<~2–3 wt%) of serpentine minerals were detected in only one place in the SAFOD borehole at depths of 3322 to 3353 m MD. This is near the center of an ~ 200-m-wide low-velocity zone identified as the principal damage zone of the San Andreas Fault [*Hickman et al.*, 2005; *Boness and Zoback*, 2005] and is also in close proximity to a place where the casing is actively deforming [*Zoback et al.*, 2005]. Due to overlap of diagnostic serpentine mineral peaks with peaks from other phases on XRD patterns it is not possible to uniquely characterize the serpentine mineral that was present in the cuttings. Based on morphologies observed using a binocular microscope, however, the serpentine minerals are lizardite and chrysotile.

3.5. Fault Zone Mineral Assemblages

[12] As discussed above, faults inferred from cuttings correspond to faults inferred from geophysical logs (Boness and Zoback, submitted manuscript, 2006). Fault zone mineral assemblages are shown in Figure 2. The 1360 m fault contains few clays (4–15 wt% combined chlorite, illite and I-S), abundant quartz (30–35 wt%) and feldspars (43–54 wt%) and a comparatively great amount of laumontite (6–13 wt%) with trace amounts of calcite. The 1926 m fault contains 1–6 wt% clay minerals, 1–4 wt% laumontite, and is quartz (62–72 wt%) and feldspar (24–33 wt%) rich. The 2545 m fault contains 22–44 wt% clay minerals, including an anomalously high percentage of mixed-layer clays (9–14% I-S), 20–27 wt% feldspars, 36–47 wt% quartz, up to 3 wt% calcite, and no detectable laumontite. Plucked grains from fault rock, identified by the presence of polished surfaces with slickensides, in this zone contain up to 61 wt% clay minerals. The 3067 m fault has up to 62–69 wt% clay minerals with the clay phase dominated by illite (48–51 wt%) and I-S (14–18 wt%), and contains no detectable laumontite. The 3300 m fault has between 14–60 wt% clays, up to 6 wt% calcite, trace amounts of laumontite (less than 2wt%), and trace amounts of serpentine minerals (less than 2–3 wt%).

[13] Work to more fully characterize the observed clay phases is ongoing. Transmission electron microscopy (TEM) of a sample from 3067 m confirms the presence of neoformed fault-related illite and mixed-layer I-S. As discussed by *Schleicher et al.* [2006], the grain-scale coatings of smectite seen in this TEM image could be significant in controlling the mechanical behavior of several of the clay-rich fault zones encountered during SAFOD drilling.

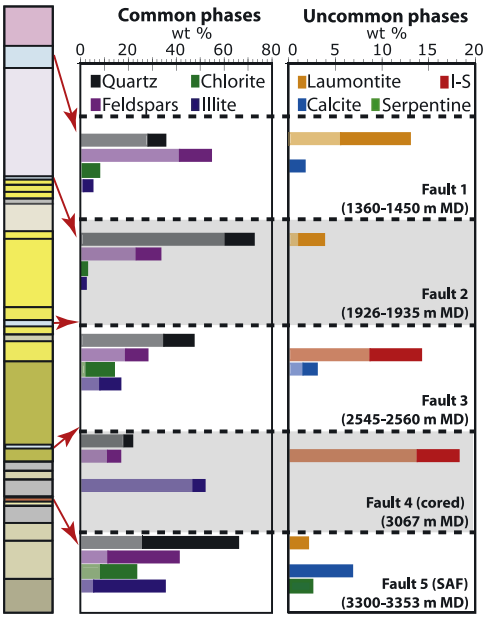

Figure 2. Mineral assemblages from XRD analyses of five major faults that were penetrated by SAFOD, including one currently active (3300–3353 m MD) member of the San Andreas Fault system. The darker portion of each bar represents the range of mineral weight percentages observed in a particular fault zone.

4. Discussion

[14] A borehole lithology section showing the geology in the local region of the SAFOD borehole is shown in Figure 3. Pre-drilling models of the subsurface of the SAFOD site are presented by *Unsworth et al.* [2000], *Rymer et al.* [2003], *McPhee et al.* [2004], and *Thurber et al.* [2004]. Post-drilling models are presented by *Thayer and Arrowsmith* [2005], *Draper et al.* [2005], *Evans et al.* [2005], and *Malin et al.* [2006].

[15] The changes in mineralogy discussed above correlate with changes in physical properties determined from geophysical logs [*Hickman et al.*, 2005; Boness and Zoback, submitted manuscript, 2006] and with an approximately 15-m-wide zone of ongoing casing deformation that is most intense at 3303 m MD [*Zoback et al.*, 2005]. These findings indicate that cuttings analyses reveal real lithologic boundaries. Moreover the comparison of plucked grains (representing sheared fault rocks) to bulk samples from the shear zone at 2545 m indicate that, while the mineralogical signature of fault rocks may be diluted in cuttings, it is nevertheless preserved.

[16] Both smectite and serpentine minerals have been used to explain the low long-term strength and mechanical behavior of the SAF [e.g., *Morrow et al.*, 1984; *Moore et al.*, 1997]. Serpentine minerals, in particular, are frequently observed at the surface in association with the SAF in

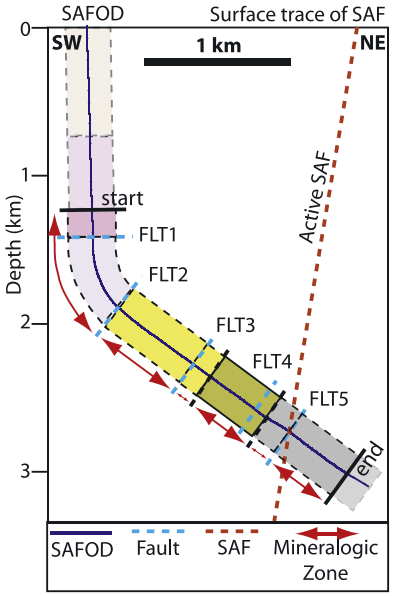

Figure 3. Limited schematic cross section along the trajectory of the SAFOD main hole. Mineralogical zones described in the text are denoted by red arrows. Boundaries between mineralogical zones are shown as either dashed blue lines (representing a confirmed fault) or dashed black lines (representing a contact of unknown origin). Faults described in Figure 2 are also labeled. The orientation of all faults and contacts are arbitrarily assigned as perpendicular to the trajectory of the SAFOD hole. "Start" and "end" denote the extent of the main hole that was analyzed in this study. Lithologies outside that range are inferred from the mud log. The active SAF is defined by connecting the region of active casing deformation to the surface trace of the active SAF.

central California [*Irwin*, 1990] and might be important in facilitating fault creep [*Moore et al.*, 1997; *Reinen*, 2000; *Andreani et al.*, 2005]. The smectites in the SAFOD Main Hole occur as a mixed-layer phase and while frictional properties have not yet been fully evaluated, faults containing these phases are relatively weak (coefficient of friction ~0.4–0.5 for bulk cuttings, ~0.33 for plucked clay-rich fault rocks (S. Tembe et al., Frictional strength of cuttings and core from SAFOD Drillhole Phases 1 and 2, submitted to *Geophysical Research Letters*, 2006).

[17] The region with the most intense casing deformation occurs ~19 m above the first appearance of serpentine in the cuttings (see Figure 1). The mechanical significance of serpentine encountered during drilling of SAFOD and its spatial relationship to active traces of the San Andreas Fault will not be known with certainty until continuous core is obtained within and adjacent to the active traces of the SAF in the final phase of SAFOD [see *Hickman et al.*, 2004].

[18] Chlorite is a common mineral in some exhumed members of the SAF system [*Chester and Chester*, 1998; *Schulz and Evans*, 1998; *Solum et al.*, 2003] and occurs in at least one shear zone from the SAFOD pilot hole [*Solum and van der Pluijm*, 2004]. Whereas chlorite appears in some fault rocks in the SAFOD main hole, it is not ubiquitous. It is most useful as an indicator of changes in lithology within fine-grained rocks, such as those encountered from ~3150 m to the bottom of the hole, indicating a distinctly different mineralogy for the sedimentary rocks on opposite sides of the actively creeping fault trace.

[19] Laumontite was observed in the Cajon Pass borehole [*Vincent and Ehlig*, 1988; *James and Sliver*, 1988] and has been described along the San Gabriel Fault [*Evans and Chester*, 1995], and in the Punchbowl Fault [*Chester and Chester*, 1998; *Schulz and Evans*, 1998; *Solum et al.*, 2003], although it is not associated with the Cocktail Fault, an older member of the Punchbowl fault system (*Solum et al.* [2003] incorrectly referred to as the Punchbowl Fault-proper in that paper). The occurrence of laumontite in fault rocks from the upper part of the SAFOD Main Hole (i.e., faults 1, 2, and 3) correlates with the occurrence of laumontite in the protolith adjacent to those faults. In addition, laumontite is present in trace amounts in the active trace of the SAF (the fault associated with casing deformation at ~3300 m MD) but is absent in the intensely sheared fault zone cored at 3067 m MD. This suggests that in this setting laumontite may not necessarily be fault related and that instead its occurrence may reflect mineralization associated with fluid flow in zones bounded by sealing faults.

5. Conclusions

[20] The purpose of this paper is to provide a first description and analysis of the mineral assemblages of the protolith and fault rocks penetrated by the SAFOD Main Hole. The mineralogic zones recognized in SAFOD are:

[21] 1. Granite/granodiorite (1200–1920 m), with bulk mineralogy of quartz + biotite ± hornblende + albite ± microcline. Alteration minerals are chlorite and laumontite. The granite and granodiorite are in fault contact at 1360 m.

[22] 2. Arkosic sedimentary rocks (1920–2550 m). Bulk mineralogy is quartz + albite ± microcline + feldspars + illite ± minor hornblende, with minor laumontite toward the top of the sequence. This suite is in fault contact with both the overlying granodiorite and the underlying sedimentary package.

[23] 3. Illite-Smectite zone (2550–2720 m). Bulk mineralogy is quartz + illite + chlorite + illite. Illite-smectite, interpreted to be a secondary fault-related phase, is common. At least one prominent fault exists in this interval and separates it from the underlying arkose.

[24] 4. Arkosic sedimentary rocks with interbedded shales (2720–3150 m). These rocks are similar to the shallower arkose occurrence, but are generally richer in illite. Laumontite is common, and is possibly associated with alteration caused by a fluid reservoir confined by sealing faults.

[25] 5. Shale/siltstone (3150–3350 m). Bulk mineralogy is chlorite + illite ± illite-smectite + quartz + albite ± microcline. Likely in fault contact with under and overlying units. Serpentine is present in small amounts in this interval.

[26] 6. Shale/siltstone (3350–3800 m). Bulk mineralogy is chlorite + illite ± illite-smectite + quartz + albite ± microcline. This zone is characterized by a mostly homogeneous population of chlorite at a significantly greater concentration than in the overlying zone.

[27] Fault zones penetrated during drilling contain a variety of mineral assemblages. The ratio of clay to non-clay phases in fault rocks is highly variable, and the greatest clay/non-clay ratio is for the cored fault zone at 3067 m. This suggests that, while fault related clays are preserved in drill cuttings, they are diluted. Both smectite and serpentine minerals occur in association with faults from the SAFOD borehole and, in particular, the sole occurrence of serpentine was in close association with a zone exhibiting active casing deformation centered at 3303 m. However, owing primarily to the poor spatial resolution of cuttings analysis, the origin, frictional properties, and relation of this serpentine (as well as potentially localized concentrations of clay minerals) to active traces of the SAF have not yet been fully established. Further study of these zones and topics will begin after continuous coring in 2007, which will be guided in part by the mineralogical observations described here.

[28] **Acknowledgments.** This work was funded by the USGS Mendenhall Program (JGS) and by the National Science Foundation, grant EAR-0446572 (BvdP) and EAR-0454525 (JPE). The SAFOD Science Team and the student volunteers are heartily thanked for their help. Nick Hayman and an unidentified reviewer are thanked for their useful reviews.

References

Andreani, M., A. M. Boullier, and J. P. Gratier (2005), Development of schistosity in a Californian serpentinite gouge, *J. Struct. Geol.*, *27*, 2256–2267.

Barton, D., K. K. Bradbury, J. G. Solum, and J. Evans (2005), Structural and lithologic characterization of the SAFOD Pilot Hole and Phase One Main Hole, *Eos Trans. AGU*, *86*(52), Fall Meet. Suppl., Abstract T21A-0451.

Boness, N. L., and M. D. Zoback (2004), Stress-induced seismic velocity anisotropy and physical properties in the SAFOD pilot hole in Parkfield, CA, *Geophys. Res. Lett.*, *31*, L15S17, doi:10.1029/2003GL019020.

Boness, N. L., and M. D. Zoback (2005), Shear velocity anisotropy in and near the San Andreas Fault: Implications for mapping stress orientations, *Eos Trans. AGU*, *86*(52), Fall Meet. Suppl., Abstract T23E-03.

Boness, N. L., and M. D. Zoback (2006), A multi-scale study of the mechanisms controlling shear velocity anisotropy in the San Andreas Fault Observatory at Depth, *Geophysics*, *71*, F131–F146, 10.1190/1.2231107.

Chester, F. M., and J. S. Chester (1998), Ultracataclasite structure and friction processes of the Punchbowl fault, San Andreas system, California, *Tectonophysics*, *295*, 199–221.

Draper, S. D., N. L. Boness, and J. P. Evans (2005), Source and significance of the sedimentary rocks in the SAFOD borehole: Preliminary analysis, *Eos Trans. AGU*, *86*(52), Fall Meet. Suppl., Abstract T24B-02.

Evans, J. P., and F. M. Chester (1995), Fluid-rock interaction in faults of the San Andreas system: Inferences from San Gabriel Fault rock geochemistry and microstructures, *J. Geophys. Res.*, *100*, 13,007–13,020.

Evans, J. P., D. E. Moore, D. Kirschner, and J. G. Solum (2005), Lithologic characterization of the deep portion of the SAFOD drillhole, *Eos Trans. AGU*, *86*(52), Fall Meet. Suppl., Abstract T21A-0450.

Hickman, S. H., R. H. Sibson, and R. Bruhn (1995), Introduction to special section: Mechanical involvement of fluids in faulting, *J. Geophys. Res.*, *100*, 12,831–12,840.

Hickman, S., M. Zoback, and W. Ellsworth (2004), Introduction to special section: Preparing for the San Andreas Fault Observatory at depth, *Geophys. Res. Lett.*, *31*, L12S01, doi:10.1029/2004GL020688.

Hickman, S. H., M. D. Zoback, and W. L. Ellsworth (2005), Structure and composition of the San Andreas Fault Zone at Parkfield: Initial results from SAFOD Phases 1 and 2, *Eos Trans. AGU*, *86*(52), Fall Meet. Suppl., Abstract T23E-05.

Irwin, W. P. (1990), Geology and plate tectonic development, in *The San Andreas Fault System, California*, edited by R. E. Wallace, *U.S. Geol. Surv. Prof. Pap.*, *1515*, 61–80.

James, E. W., and L. T. Sliver (1988), Implications of zeolites and their zonation in the Cajon Pass deep drillhole, *Geophys. Res. Lett.*, *15*, 973–976.

Lachenbruch, A. H., and J. H. Sass (1992), Heat flow from Cajon Pass, fault strength, and tectonic implications, *J. Geophys. Res.*, *97*, 4995–5015.

Malin, P., E. Shalev, H. Balven, and C. Lewis-Kenedi (2006), Structure of the San Andreas Fault at SAFOD from P-wave tomography and fault-guided wave mapping, *Geophys. Res. Lett.*, *33*, L13314, doi:10.1029/2006GL025973.

McPhee, D., R. Jachens, and C. Wentworth (2004), Crustal structure across the San Andreas Fault at the SAFOD site from potential field and geologic studies, *Geophys. Res. Lett.*, *31*, L12S03, doi:10.1029/2003GL019363.

Moore, D. E., D. A. Lockner, M. Shengli, R. Summers, and J. D. Byerlee (1997), Strengths of serpentinite gouges at elevated temperatures, *J. Geophys. Res.*, *102*, 14,787–14,801.

Morrow, C. A., L. Q. Shi, and J. D. Byerlee (1984), Permeability of fault gouge under confining pressure and shear stress, *J. Geophys. Res.*, *89*, 3193–3200.

Reinen, L. A. (2000), Seismic and aseismic slip indicators in serpentinite gouge, *Geology*, *28*, 135–138.

Rymer, M. J., R. D. Catchings, and M. R. Goldman (2003), Structure of the San Andreas fault zone as revealed by surface geologic mapping and high-resolution seismic profiling near Parkfield, California, *Geophys. Res. Abstr.*, *5*, 13,523.

Schleicher, A. M., B. A. van der Pluijm, J. G. Solum, and L. N. Warr (2006), The origin and significance of clay minerals on surfaces, in fractures and in veins from SAFOD borehole samples (Parkfield, California), *Geophys. Res. Lett.*, *33*, L16313, doi:10.1029/2006GL026505.

Schulz, S. E., and J. P. Evans (1998), Spatial variability in microscopic deformation and composition of the Punchbowl Fault, southern California: Implications for mechanisms, fluid-rock interaction, and fault morphology, *Tectonophysics*, *295*, 223–244.

Solum, J. G., and B. A. van der Pluijm (2004), Phyllosilicate mineral assemblages of the SAFOD Pilot Hole and comparison with an exhumed segment of the San Andreas Fault System, *Geophys. Res. Lett.*, *31*, L15S19, doi:10.1029/2004GL019909.

Solum, J. G., B. A. van der Pluijm, D. R. Peacor, and L. N. Warr (2003), The influence of phyllosilicate mineral assemblages, fabrics, and fluids on the behavior of the Punchbowl Fault, southern California, *J. Geophys. Res.*, *108*(B5), 2233, doi:10.1029/2002JB001858.

Thayer, M., and R. Arrowsmith (2005), Fault zone structure of Middle Mountain, central California, *Eos Trans. AGU*, *86*(52), Fall Meet. Suppl., Abstract T21A-0458.

Thurber, C., S. Roecker, H. Zhang, S. Baher, and W. Ellsworth (2004), Fine-scale structure of the San Andreas fault zone and location of the SAFOD target earthquakes, *Geophys. Res. Lett.*, *31*, L12S02, doi:10.1029/2003GL019398.

Unsworth, M., P. Bedrosian, M. Eisel, G. Egbert, and W. Siripunvaraporn (2000), Along strike variations in the electrical structure of the San Andreas Fault at Parkfield, California, *Geophys. Res. Lett.*, *27*, 3021–3024.

Vincent, M. W., and P. L. Ehlig (1988), Laumontite mineralization in rocks exposed of San Andreas Fault at Cajon Pass, southern California, *Geophys. Res. Lett.*, *15*, 977–980.

Zoback, M. D. (2000), Strength of the San Andreas fault, *Nature*, *405*, 31–32.

Zoback, M. D., S. Hickman, and W. Ellsworth (2005), Overview of SAFOD Phases 1 and 2: Drilling, sampling and measurements in the San Andreas Fault zone at seismogenic depth, *Eos Trans. AGU*, *86*(52), Fall Meet. Suppl., Abstract T23E-01.

J. P. Evans, Department of Geology, Utah State University, 4505 Old Main Hill, Logan, UT 84322-4505, USA.

S. H. Hickman, D. A. Lockner, D. E. Moore, and J. G. Solum, Earthquake Hazards Team, U.S. Geological Survey, 345 Middlefield Road, MS 977, Menlo Park, CA 94025, USA. (jsolum@usgs.gov)

A. M. Schleicher and B. A. van der Pluijm, Department of Geological Sciences, University of Michigan, 1100 N. University Ave., 2534 C.C. Little Bldg., Ann Arbor, MI 48109, USA.